Energy spectrum and structure of confined one-dimensional few-electron systems with and without coupling to light in a cavity

Chenhang Huang, Daniel Pitagora, Timothy Zaklama, and Kálmán Varga*
Department of Physics and Astronomy, Vanderbilt University, Nashville, Tennessee 37235, USA

(Received 20 July 2021; accepted 4 October 2021; published 21 October 2021)

An explicitly correlated Gaussian basis is used to calculate the energies and wave functions of one-dimensional few-electron systems in confinement potentials created by external potentials or coupling to light in cavity. The appearance and properties of electron density peaks as the function of the relative strength of the confinement and the Coulomb interaction are studied. It is shown that similar Wigner crystal-like structures can be formed by coupling electrons to light due to the dipole self-interaction term in the light-matter Hamiltonian, provided an additional extremely weak confining potential is present. The relation of these systems to Wigner crystals is discussed.

DOI: 10.1103/PhysRevA.104.043109

I. INTRODUCTION

A Wigner crystal is a solid phase of electrons, predicted by Wigner in 1934 [1]. If an electron gas has a low enough density in a uniform, neutralizing background, the system can crystallize through the formation of an electron lattice, driven by Coulomb interaction.

The experimental study of Wigner crystals is hindered by the fact that low electron densities have to be reached in the presence of defects and impurities. Nevertheless, Wigner crystals have been experimentally demonstrated in liquid helium [2] and semiconductor heterostructures [3,4]. These experiments have led to intense theoretical work focusing on energetics and structures of Wigner crystals [5–13].

Recently, there has been renewed interest in Wigner crystals after experimentally imaging them in Moire superlattices [14–16] and one-dimensional (1D) systems [17–19]. These new systems emerge as a highly conductive platform to study strong electronic correlations as well as topology. The most interesting experimental example of 1D Wigner crystals is found by real-space imaging the density profile of electrons confined in carbon nanotubes [18]. The Wigner lattice formation of bipolarons in conducting polymer nanowires has also been studied recently [20]. The experimental observations have generated renewed theoretical interest in one-dimensional Wigner crystals [21,22].

The real-space imaging revealed the signatures of few-electron Wigner crystals in 1D systems [18] in the form of charge density peaks, and the number of peaks found to be equal to the number of electrons. This picture is explained by the effect of strong Coulomb interaction [18]. If there is no interaction, then electrons populate the particle in the box states. For example, in the case of two electrons with one spin up and one spin down, the two electrons can occupy the lowest particle in the box eigenstate, resulting in one density peak. In the case of strong Coulomb interaction, a different picture is expected to emerge: the Coulomb repulsion keeps the two electrons apart and two density peaks appear. The same is true for N electrons, i.e., the number of peaks is equal to the number of electrons [18]. The question is what the role of the symmetry of the correlated few-electron wave function is in the formation of the density peaks. Is the Coulomb repulsion the dominant factor or does the Pauli correlation dictated by the antisymmetry requirement also play a substantial role?

In this work, we will investigate the role of the electronic correlations and long-range Coulomb interactions in the energy and structure of confined 1D few-electron systems using explicitly correlated basis functions. We will study the limit between the regions where these systems can be considered to be Wigner crystals (where the Coulomb interaction is dominant) and strongly correlated 1D systems (where the confinement and the Pauli correlations determine the structure).

One-dimensional Wigner crystals have been studied using the bosonization method [23], with an effective Hamiltonian [24] and the configuration interaction (CI) approach [21]. Quantum Monte Carlo (QMC), including diffusion quantum Monte Carlo, methods are also frequently used to calculate the properties of Wigner crystals [8,25–28]. The advantage of the QMC approaches is that they can be relatively easily extended to systems with a larger number of electrons. See a recent review highlighting other approaches in Ref. [29]. In this paper, we complement these works with a more accurate approach that includes the full Coulomb Hamiltonian, using correlated basis functions to avoid the convergence issues of CI calculations, and addresses the structure of spin configurations.

In this work, we refer to the crystal-like arrangement of electrons that minimizes the Coulomb interaction energy as Wigner crystals if the electron density is significantly different from the electron density determined by the confining potential alone—in other words, if the Coulomb energy is dominant. A stringent definition of Wigner crystallization would involve a critical density where the potential energy of the system starts to dominate over the kinetic energy. In the few-electron systems considered here, this critical density

*kalman.varga@vanderbilt.edu

 ©2021 American Physical Society

or phase transition from a fluid to a crystalline phase cannot be easily identified. Wigner crystallization in terms of a phase transition in 1D systems is studied and nicely explained in Refs. [21,22].

The Wigner crystals are formed in external confining potentials. An alternative possibility to confinement is the use of electron interactions with cavity photons. The dipole self-polarization term $\frac{1}{2}(\vec{\lambda}\cdot\vec{R})^2$ (where $\vec{\lambda}$ is the interaction strength and $\vec{R}$ is the dipole moment) of the light-matter interaction Hamiltonian creates a harmonic-oscillator-like confinement. We will show that coupling a very weakly confined few-electron system to light in cavity leads to tightly localized Wigner crystal-like structures. Such systems have not yet been experimentally discovered, but carbon nanotubes have been studied in microwave cavities [30], and coherent spin states in carbon nanotubes coupled to cavity photons have been investigated [31]. Other 1D systems confined in parabolic potentials [32] or 1D optical lattices in cavity [33] have also been studied.

1D systems have been used as test cases mimicking more complicated dynamics because numerical solutions are easier in 1D. This interest is intensified with the investigation of light-matter coupling, where the representation of the coupled light-matter wave function requires the high-dimensional product of spatial and photon bases. Restricting the nuclear or electronic motion to 1D makes model calculations feasible [34–40]. Our calculations might help to improve these 1D model calculations and extend them to more complicated cases.

The ground-state energies and wave functions will be calculated using explicitly correlated Gaussian (ECG) basis functions [41]. The basis parameters have been optimized using the stochastic variational method (SVM) [42]. The advantage of the approach is that the matrix elements are analytically available [6,42,43] and it produces very accurate energies and wave functions [41]. This method has been used to describe excitonic complexes [8,41,44–47], and two- and three-dimensional quantum dots [48,49].

We will compare our results to density functional theory (DFT) [50,51] calculations. Spin-polarized DFT calculations have often been used to analyze the structure and energetics of two-dimensional confined electron systems and Wigner crystals [52–57]. In this work, we will investigate how well the DFT densities approximate the accurate few-particle results. The advantage of the DFT is that it can easily be extended for larger systems, while our ECG approach scales with $N!$ due to the explicit antisymmetrization of the N electron wave function, which reduces the application to small systems.

II. FORMALISM

A. Few-electron system in an external confining potential in 1D

The Hamiltonian of an N electron system interacting with a Coulomb interaction and confined in an external potential V_c reads

$$H_e = -\frac{1}{2}\sum_{i=1}^{N}\frac{\partial^2}{\partial x_i^2} + \sum_{i<j}^{N} V(x_i, x_j) + \sum_{i=1}^{N} V_c(x_i), \tag{2.1}$$

where x_i is the coordinate of the ith electron, and atomic units are used. Due to the singular nature of the Coulomb potential, a soft Coulomb potential will be used,

$$V(x_i - x_j) = \frac{1}{\sqrt{(x_i - x_j)^2 + a^2}}, \tag{2.2}$$

and the confining potential is a quadratic $V_c(x) = \frac{1}{2}\omega^2 x^2$ potential. Similar potentials are used in Ref. [21]. The softening parameter a was chosen to be $a = 1$. This is a typical choice in calculations using numerical grids allowing relatively large (0.1 a.u.) grid spacing. The results of the calculations are not sensitive to this parameter provided that it is not very small ($a \ll 1$). Very small values lead to prohibitively small grid spacing in the DFT calculations.

The wave function is expanded into ECGs of the form

$$\psi_k(\vec{x}) = \mathcal{A}\left\{e^{-\frac{1}{2}\sum_{i<j}^{N}\alpha_{ij}^k (x_i - x_j)^2} e^{-\sum_{i=1}^{N}\beta_i^k (x_i - s_i^k)^2}\chi_S\right\}, \tag{2.3}$$

where $\vec{x} = (x_1, \ldots, x_n)$, $\mathcal{A}$ is an antisymmetrizer, χ_S is the N electron spin function (coupling the spin to S), and α_{ij}^k, β_i^k, and s_i^k are nonlinear parameters (k stands for the kth set of parameters). The

$$e^{-\beta_i (x_i - s_i)^2} \tag{2.4}$$

function is a Gaussian shifted into position s_i. By optimizing the center s_i and the width β_i, one can describe the position of particle i. The

$$e^{-\frac{1}{2}\sum_{i<j}^{N}\alpha_{ij}(x_i - x_j)^2} \tag{2.5}$$

part can be used to represent the correlation between particles i and j. The N particle wave function then can be written as

$$\Psi(\vec{x}) = \sum_{k=1}^{K} c_k \psi_k(\vec{x}), \tag{2.6}$$

where K is the dimension of the basis. The linear coefficients c_k can be determined by diagonalization, and the nonlinear ones are optimized by the SVM. In the SVM, the nonlinear parameters are optimized by randomly generating a large number of candidates and selecting the ones that give the lowest energy [41,42]. The size of the basis can be increased by adding the best states one by one and a K-dimensional basis can be refined by replacing states with randomly selected better basis functions. This approach is very efficient in finding suitable parameters in high-dimensional spaces.

B. Few-electron system in 1D coupled to photons in cavity

In this case, the Hamiltonian is given by

$$H = H_e + H_{ph} = H_e + H_p + H_{ep} + H_d. \tag{2.7}$$

H_{ph} describes the electron-photon interaction and H_e is the same electronic Hamiltonian as in the previous section. The electron-photon interaction can be described using the Pauli-Fierz (PF) nonrelativistic QED Hamiltonian. The PF Hamiltonian can be rigorously derived [39,58–61] by applying the Power-Zienau-Woolley gauge transformation [42], with a unitary phase transformation on the minimal coupling

$(p \cdot A)$ Hamiltonian in the Coulomb gauge,

$$H_{ph} = \frac{1}{2}\sum_{\alpha=1}^{M}\left[-\frac{\partial^2}{\partial p_\alpha^2} + (\omega_\alpha p_\alpha - \lambda_\alpha X)^2\right], \tag{2.8}$$

where $X = \sum_{i=1}^{N} q_i x_i$ is the dipole operator ($q_i = -1$ is the electron charge). This Hamiltonian describes M photon modes with elongation p_α, frequency ω_α, and polarization λ_α. The sum can be decomposed into the sum of a photonic part H_p, dipole self-interaction H_d, and H_{ep} that describes the light-matter interaction in the electric-dipole form. The photonic part is

$$H_p = \sum_{\alpha=1}^{M}\left(-\frac{1}{2}\frac{\partial^2}{\partial p_\alpha^2} + \frac{\omega_\alpha^2}{2}p_\alpha^2\right) = \sum_{\alpha=1}^{M}\omega_\alpha\left(a_\alpha^+\hat{a}_\alpha + \frac{1}{2}\right), \tag{2.9}$$

where $\hat{a}_\alpha = \sqrt{\frac{\omega_\alpha}{2}}(p_\alpha - \frac{1}{\omega_\alpha}\frac{\partial}{\partial p_\alpha})$ is the annihilation operator and $\hat{a}_\alpha^+ = \sqrt{\frac{\omega_\alpha}{2}}(p_\alpha + \frac{1}{\omega_\alpha}\frac{\partial}{\partial p_\alpha})$ is the creation operator. With the introduction of the creation and annihilation operators, the photon states $|n_\alpha\rangle$ can be generated by multiple applications of the creation operators on the vacuum state $n_\alpha = (\hat{a}_\alpha^+)^n|0\rangle$, and all other photon operations can be done using $\hat{a}_\alpha$ and $\hat{a}_\alpha^+$. The interaction term is

$$H_{ep} = -\sum_{\alpha=1}^{M}\omega_\alpha p_\alpha \lambda_\alpha X = -\sum_{\alpha=1}^{M}\sqrt{\frac{\omega_\alpha}{2}}(\hat{a}_\alpha + \hat{a}_\alpha^+)\lambda_\alpha X. \tag{2.10}$$

Note that $\hat{a}_\alpha$ and $\hat{a}_\alpha^+$ only connect photon state $|n_\alpha\rangle$ to $|n_\alpha \pm 1\rangle$, and the matrix elements of the dipole operator X are only nonzero between spatial basis functions of angular momentum l and $l \pm 1$. The strength of the electron-photon interaction is described by the effective coupling parameter

$$g_\alpha = |\lambda_\alpha|\sqrt{\frac{\omega_\alpha}{2}}. \tag{2.11}$$

The dipole self-interaction is

$$H_d = \frac{1}{2}\sum_{\alpha=1}^{M}(\lambda_\alpha X)^2, \tag{2.12}$$

which describes how the polarization of the electrons acts back on the photon field. The importance of this term for the existence of a ground state is discussed in Ref. [58].

We will only consider one photon mode, and the wave function in this case will be defined as

$$\Psi(\vec{x}) = \sum_{n}\sum_{k=1}^{K_n} c_k \psi_k^n(\vec{x})|n\rangle, \tag{2.13}$$

where ψ_k^n is the spatial basis function belonging to an n photon state and $|n\rangle$ is the photon state. The summation over n includes photon states that significantly lower the energy. K_n is the dimension of the basis belonging to photon state $|n\rangle$.

The necessary matrix elements can be analytically calculated for both the spatial and the photon parts. Note that the basis functions in Eq. (2.3) do not have definite angular momentum quantum numbers. During the optimization, the symmetry of the Hamiltonian will dictate the selection of basis functions with appropriate symmetry. For example, if the Hamiltonian is spherically symmetric (which is not true in the present case due to the interaction with the photons), then the wave function converges to $L = 0$ angular momentum for the lowest state. In principle, one can use Wigner rotation matrices to project out good angular momentum functions, but in our present case many angular momentum states will be coupled with the photons and we will let the SVM select the proper ground state.

C. Density functional approach

In DFT, the Hamiltonian is defined as

$$H_e = -\frac{1}{2}\frac{d^2}{dx^2} + V_H[\rho(x)] + V_{\rm ex}[\rho(x)] + V_c(x), \tag{2.14}$$

where $V_{\rm ex}$ is the exchange-correlation potential and V_H is the Hartree potential. The local density approximation (LDA) is used for the exchange-correlation potential [62] and the Hartree potential is defined as

$$V_H[\rho(x)] = \iint \rho(x')V(x-x')dx', \tag{2.15}$$

where V is the soft Coulomb potential defined in Eq. (2.2). The LDA adopted in this calculation is based on a three-dimensional homogeneous free electron gas [62]. The solution of the eigenvalue problem of the DFT Hamiltonian,

$$H_e\phi_i(x) = \epsilon_i\phi_i(x), \tag{2.16}$$

gives the Kohn-Sham orbitals and the density is calculated as

$$\rho(x) = \sum_{i=1}^{N}\phi_i(x)^2. \tag{2.17}$$

In this case, we solve the eigenvalue equation on a numerical grid with 400 grid points and 0.1 a.u. grid spacing.

III. RESULTS AND DISCUSSION

In this section, we present our numerical results. Atomic units are used. In a typical system, the electron has an effective mass

$$m_e^* = m_e m_0, \tag{3.1}$$

where m_0 is the physical mass of the electron and κ is the dielectric constant of the medium. With this, we can define an effective Bohr radius as

$$a^* = \frac{\hbar^2\kappa}{m_e^* e^2} = \frac{\kappa}{m_e}a_0, \tag{3.2}$$

where $a_0 = \frac{\hbar^2}{m_0 e^2}$ is the hydrogenic Bohr radius ($a_0 = 0.529\,177$ Å). Similarly, the effective Bohr energy reads

$$E^* = \frac{e^2}{\kappa a^*} = \frac{m_e}{\kappa^2}E_0, \tag{3.3}$$

where $E_0 = e^2/a_0$ is the Hartree energy ($E_0 = 27.211$ eV). To convert the results to eV and Å, one has to multiply the energies by E^* and the distances by a^*. In the experiment of Ref. [18], $m_e = 0.0062$ and $\kappa = 1$, which gives $a^* = 85$ Å and $E^* = 169$ meV. In this case, a harmonic-oscillator confinement with $\omega = 0.1$ a.u. corresponds to $\hbar\omega = 17.9$ meV. The unit of λ is $\sqrt{E^*}/a/*$. The weakest harmonic-oscillator

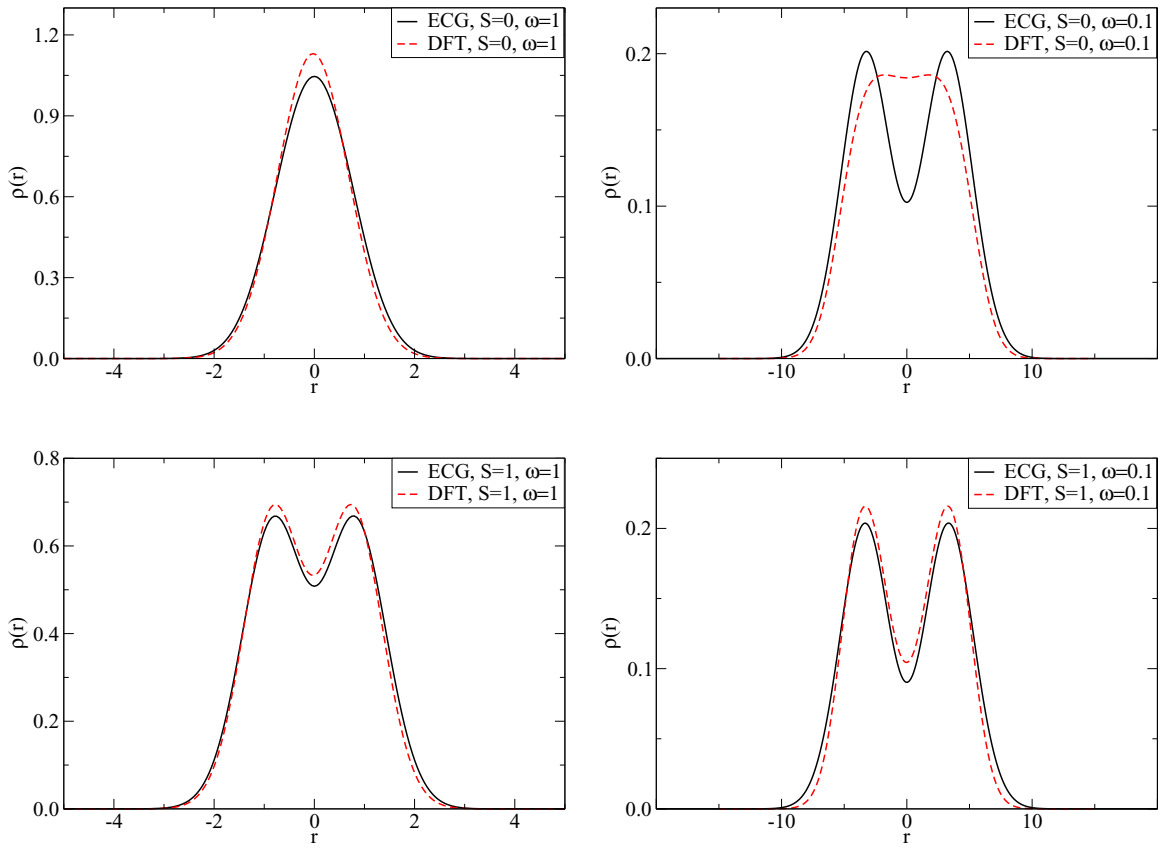

FIG. 1. Electron density of the two-electron system. Top: $S = 0$; bottom: $S = 1$. Left: $\omega = 1$; right: $\omega = 0.1$ a.u. The solid curve is calculated by ECG; the dashed line is by DFT. The distance r is in a.u.

confinement with $\omega = 0.01$ used in this work roughly corresponds to the confinement in the experiment of Ref. [18].

A. Electrons in a harmonic confinement

The DFT and ECG results are compared in Figs. 1–5 for $N = 2$–6 particle systems with different spin configurations. The ECG results are well converged and can be considered as benchmark calculations; the DFT calculations seem to provide good approximations to the electron density in certain cases. There is a very small asymmetry between the peaks of the ECG and DFT densities due to the grid resolution in the DFT calculations. We have tried two different confinement potentials. The first potential, $\omega = 1$ a.u., is strong and confines the electrons into a $[-5, 5]$ a.u. box (high electron density). The second one, $\omega = 0.1$ a.u., confines the electrons into a $[-20, 20]$ a.u. box. We also have calculations (see Supplemental Material [63]) for $\omega = 0.01$ which roughly correspond to a $[-80, 80]$ a.u. box, but the results are not significantly different from the $\omega = 0.1$ a.u. results. Besides the quadratic confinement, we have also tested quartic confinement (see Supplemental Material [63]), but we did not observe any important change in the tendencies.

The two-electron density (Fig. 1) does not show two peaks for strong confinement for $S = 0$, but the two peaks appear for the weaker case. The confinement alone would create only one peak in this system, so the appearance of the two peaks is due to the relative increase of Coulomb interaction. In the spin-polarized $S = 1$ case, we have two peaks for strong and weak confinements because the Pauli and the Coulomb repulsion together are strong enough to localize the electrons. The localization is naturally more significant in the weak confinement case, which is shown by the increased distance and the lower density between the density peaks. The two-peak structure does not disappear when the strength of the confinement increases; for $\omega = 20$ a.u., the electrons are squeezed into a $[-1, 1]$ a.u. interval, but the two peaks are present in the spin-polarized case. The reason is simple: in the case of very strong confinement, the single particle states of the confining potential determine the structure of the system and the Coulomb contribution is negligible. The two spin-polarized electrons have to occupy different orbitals: the first is the ground state and the second is the first-excited state. The ground-state single particle wave function is nodeless; the first-excited state has one node and is more extended in space than the ground state. The density, i.e., the sum of the square of the two wave functions, will always have two peaks coming from the first-excited state.

The contributions of the kinetic, Coulomb, and confinement parts to the total energy are shown in Table I. For very strong confinement ($\omega = 20$ a.u.), the lowest single particle energy of the harmonic confinement is $E_0 = \frac{1}{2}\omega = 10$ a.u., and the energy of the first-excited state is $E_1 = \frac{3}{2}\omega = 30$ a.u. As we have discussed above, for $S = 0$, the two electrons can occupy the lowest state, and the calculated kinetic energy 9.99 a.u. and the confinement energy 10.01 a.u. (for a harmonic oscillator, the kinetic and potential en-

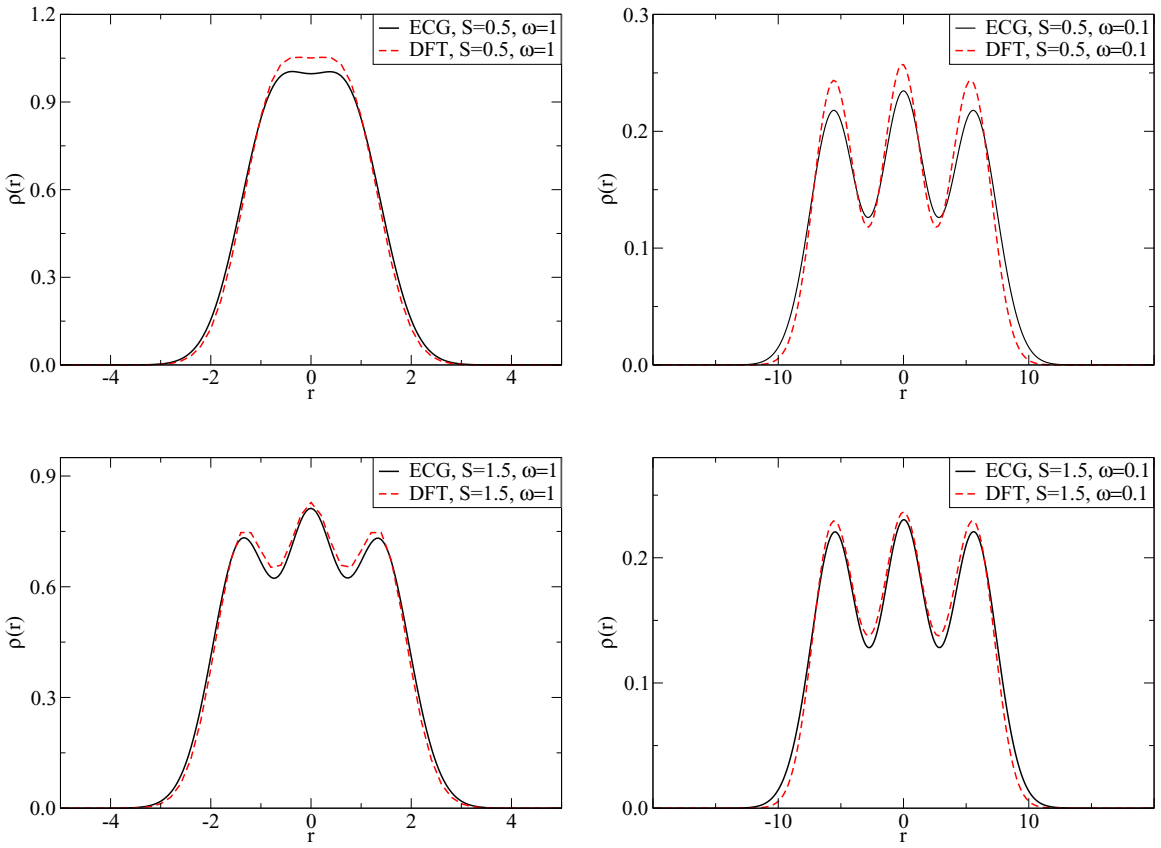

FIG. 2. Electron density of the three-electron system. Top: $S = 1/2$; bottom: $S = 3/2$. Left: $\omega = 1$ a.u.; right: $\omega = 0.1$ a.u. The distance r is in a.u. The solid curve is calculated by ECG; the dashed line is by DFT.

ergy contributions are equal according to the virial theorem) show that this is the case. For the spin-polarized case, the electrons occupy the first two states and the energy contribution is equal to 20 a.u. for the kinetic and harmonic parts. The Coulomb contribution is nearly equal in both the $S = 0$ and $S = 1$ cases, but it is very small compared to the kinetic and harmonic contributions. For $\omega = 1$ a.u., $E_0 = 0.5$ a.u., and $E_1 = 1.5$ a.u., the single particle dominance is much less, the kinetic and confinement energy contributions are not equal to 0.5 a.u. ($S = 0$) and 1 a.u. ($S = 1$), and the Coulomb energy is significant compared to the other terms. For weaker confinements, the Coulomb energy becomes the largest term (about half of the total energy) and the kinetic energy becomes very small.

TABLE I. Energy contributions (in atomic units) for a two-electron system as a function of the confinement strength. T is the kinetic energy, V is the Coulomb energy, V_c is the confinement contribution, and E is the total energy.

	ω	T	V	V_c	E
$S = 0$	0.01	0.007	0.032	0.025	0.0691
	0.1	0.07	0.017	0.014	0.39
	1.0	0.44	0.76	0.57	1.77
	20.0	9.99	0.97	10.01	20.97
$S = 1$	0.01	0.007	0.032	0.025	0.0691
	0.1	0.07	0.017	0.014	0.39
	1.0	0.92	0.54	1.09	2.55
	20.0	20.0	0.94	20.00	40.94

Similar arguments are true for spin-polarized states with $N = 3, 4, 5, 6$ electron number cases, shown in Figs. 2–5, respectively. In particular, each spin-polarized case with N particles exhibits N density peaks regardless of the confinement, for a similar reason as in the two-electron case. For example, for $N = 6$, the first six states with increasing number of nodes are occupied, each contributing to the density. However, the number of density peaks does not necessarily agree with the number of particles in mixed-spin systems and cannot be readily determined in a simple way. As before, the electron density is more localized in the stronger confinements in most cases. Quartic or other forms of confinement do not change the shapes too much and the nodal structure is still the same (see Supplemental Material [63]). This 1D picture is significantly different from the 2D or 3D cases where several single particle states are degenerate and the electrons can be placed in different spatial configurations. In 1D, the electron peaks are aligned in a line with equal spacing, while in higher dimensions, more complex crystal structures (square or trigonal lattice, concentric rings) can be formed.

Both the three- and four-electron systems can show a single peak (see Figs. 2 and 3) in mixed-spin cases if the confinement is strong. The two density peaks in the $S = 0$, $\omega = 1$ case of $N = 4$ can be easily explained. There are two electrons with up spins and two with down spins and the

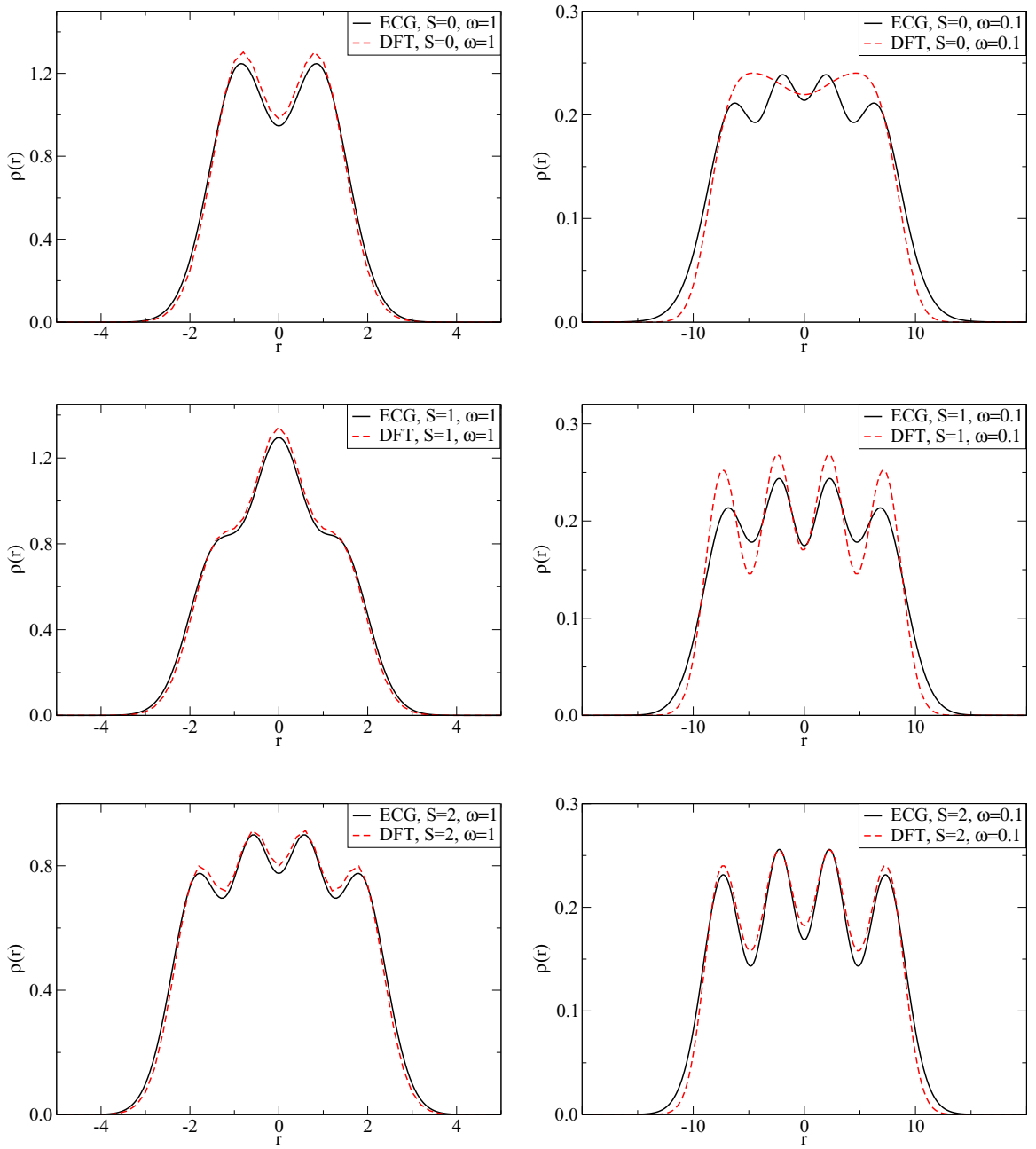

FIG. 3. Electron density of the four-electron system. Top: $S = 0$; middle: $S = 1$; bottom: $S = 2$. Left: $\omega = 1$ a.u.; right: $\omega = 0.1$ a.u. The solid curve is calculated by ECG; the dashed line is by DFT. The distance r is in a.u.

distinguishable particles can occupy the same spatial regions. In the $S = 1$, $\omega = 1$ case of $N = 4$, there is one peak with two shoulders. In this case, most likely an up-down electron pair occupies the middle region, and the two remaining electrons with spin up are on the outer region forming the shoulders.

The structure in the $N = 5$ and $N = 6$ cases can be understood using similar arguments to the $N = 3, 4$ cases. One can also think of these as a structure formed by an $N = 3$ or $N = 4$ system by adding two electrons. For example, the middle peak in the $S = 3/2$, $\omega = 1$ a.u., $N = 5$ case is very similar to the $S = 1/2$, $\omega = 1$ a.u., $N = 3$ density, with two electrons added forming the outer shoulders. The same is true for $S = 2$, $\omega = 1$ a.u., $N = 6$ compared with $S = 1$, $\omega = 1$ a.u., $N = 4$.

If the confinement gets weaker, then Wigner crystal-like structures appear. For example, three and four peaks are present for $N = 3$ and $N = 4$ electrons in the case of $\omega = 0.1$ a.u. (see Figs. 2 and 3). The confinement alone creates only one peak for $N = 3$ and two peaks for $N = 4$ (similar to the densities shown on Figs. 2 and 3 for $\omega = 1$). The Coulomb interactions lead to the appearance of three and four peaks. A similar tendency is true for larger systems, but the confinement has to be even smaller in those cases.

The DFT and ECG densities are in very good agreement for $\omega = 1$. In these cases, the densities are very similar and the

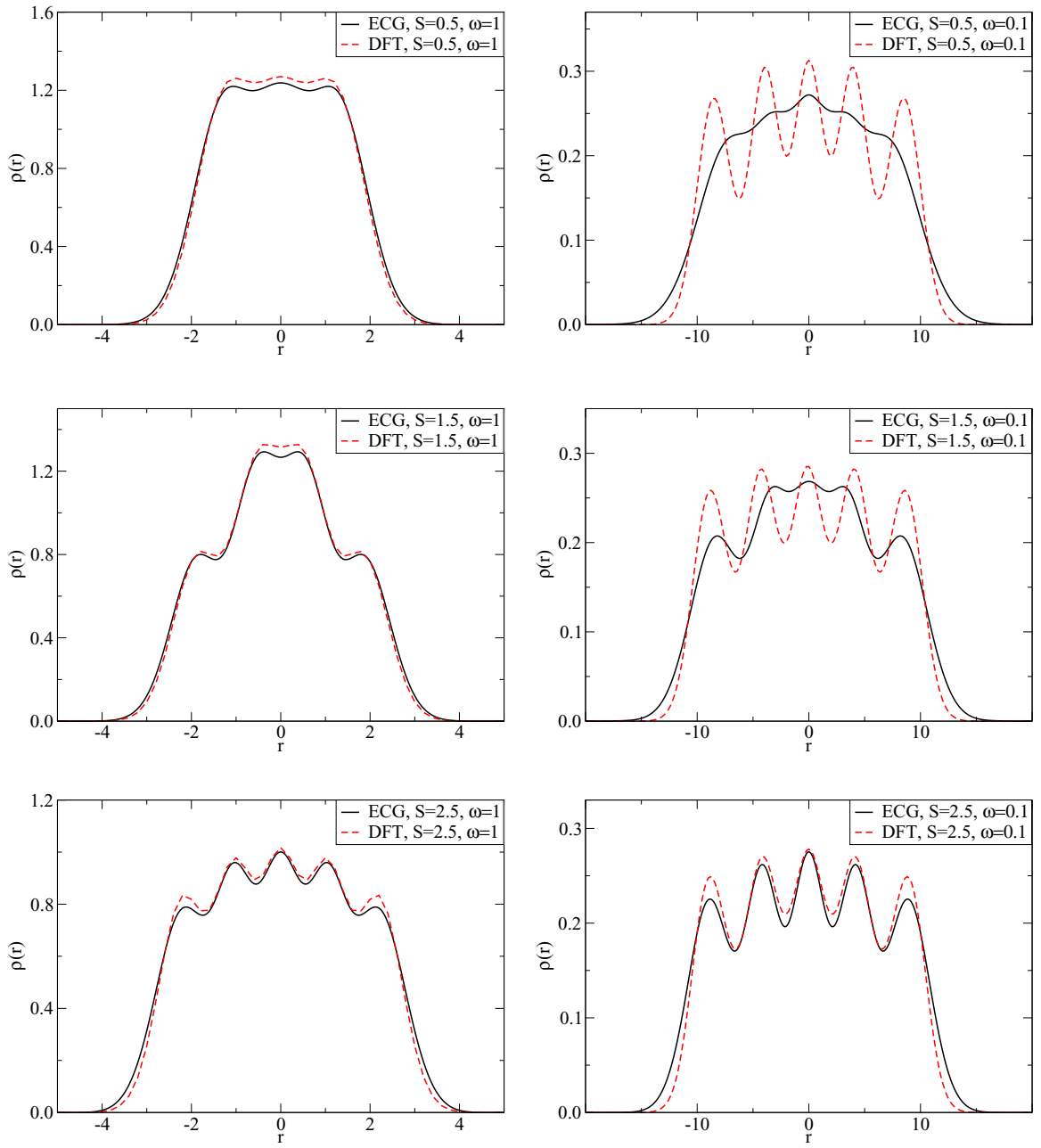

FIG. 4. Electron density of the five-electron system. Top: $S = 1/2$; middle: $S = 3/2$; bottom: $S = 5/2$. Left: $\omega = 1$ a.u.; right: $\omega = 0.1$ a.u. The solid curve is calculated by ECG; the dashed line is by DFT. The distance r is in a.u.

energies are comparable. For weaker confinements, the agreement is not as good, probably because the present LDA is not a good approximation for low densities where the Coulomb interaction plays a more pronounced role. For spin-polarized systems, the DFT density remains close to the ECG even for weaker confinements. As we have mentioned, the present LDA functional is adopted from 3D free electron gas. LDA functionals are also developed for 1D cases [64,65]. The long $1/|x|$ tail has a much more dominant effect in 1D than in 3D. This probably leads to the inaccuracy of the present DFT calculation in the weak confinement (low density) case. A 1D LDA functional [64,65] would perhaps improve the solution.

Table II shows the energy of the $N = 2$–6 systems for ECG and DFT. Besides general trends, no agreement is expected, and the DFT with LDA is not close to the accurate ECG energies for small atoms such as H and He, or for Li [41]. The general trends, however, are similar. For example, energy orders of different spin states are predicted to be the same by ECG and DFT, especially for strong confinements. One particular failure of DFT is the negative energy for the $N = 2$, $S = 1$ case, and this clearly shows that one needs to go beyond LDA. Due to the shell structure, the energies of different spin states are very different in cases of strong confinement, but for weak confinement, the energies are nearly degenerate.

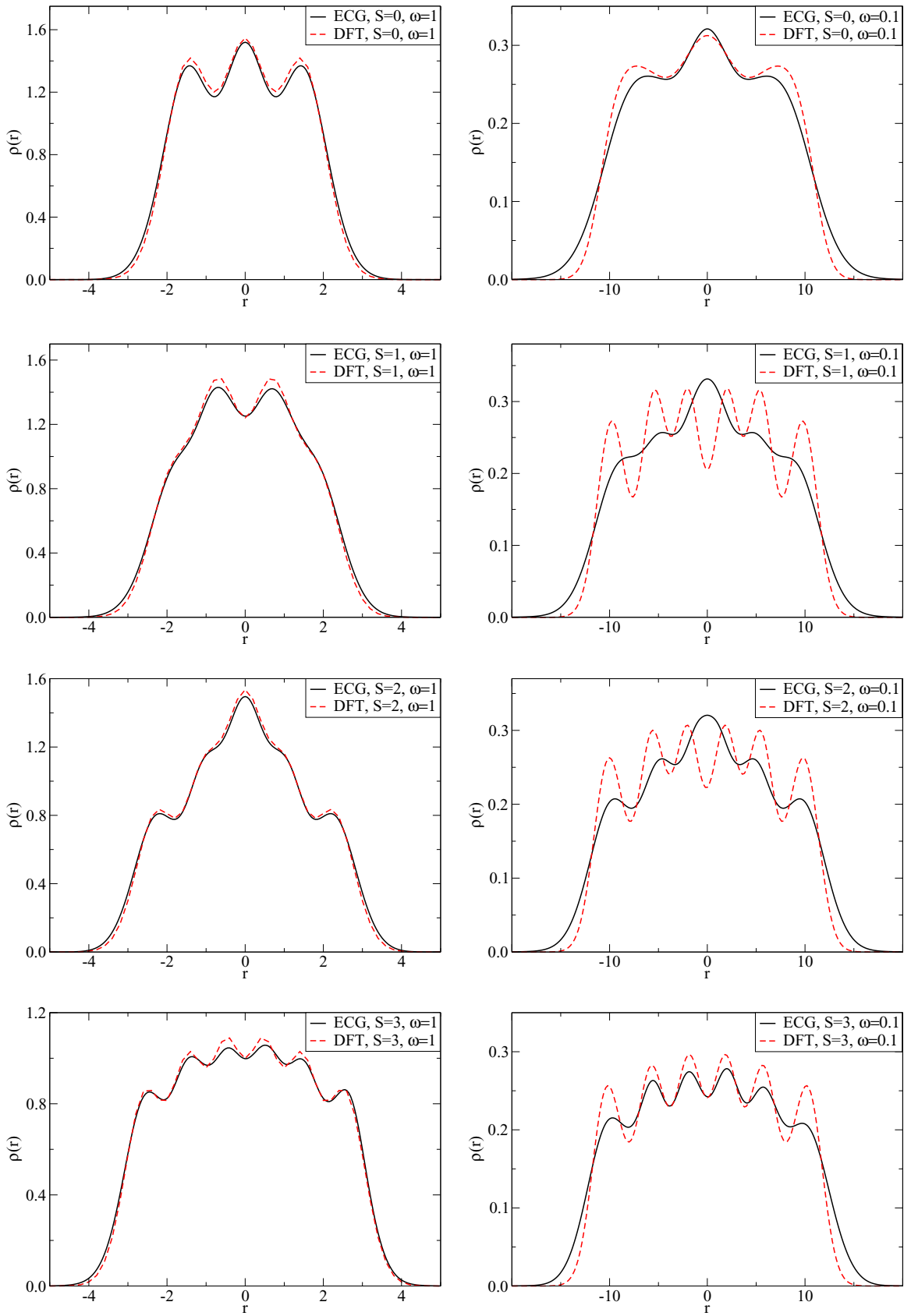

FIG. 5. Electron density of the six-electron system. Top: $S = 0$; middle: $S = 1$ and $S = 2$; bottom: $S = 3$. Left: $\omega = 1$ a.u.; right: $\omega = 0.1$ a.u. The solid curve is calculated by ECG; the dashed line is by DFT. The distance r is in a.u.

TABLE II. Total energy E (in atomic units) for few-electron systems as a function of the external confinement strength ω.

	ω	E (ECG)	E (DFT)
		$2e^-$	
$S=0$	0.1	0.392	0.005
	1.0	1.774	1.111
$S=1$	0.1	0.396	−0.1
	1.0	2.554	1.827
		$3e^-$	
$S=0.5$	0.1	1.009	0.256
	1.0	4.481	3.385
$S=1.5$	0.1	1.016	0.246
	1.0	6.078	4.872
		$4e^-$	
$S=0$	0.1	1.877	0.982
	1.0	7.808	6.261
$S=1$	0.1	1.887	0.846
	1.0	8.589	7.005
$S=2$	0.1	1.894	0.837
	1.0	11.024	9.293
		$5e^-$	
$S=0.5$	0.1	2.999	1.678
	1.0	12.490	10.443
$S=1.5$	0.1	2.985	1.671
	1.0	14.069	11.955
$S=2.5$	0.1	3.020	1.663
	1.0	17.379	15.064
		$6e^-$	
$S=0$	0.1	4.362	2.822
	1.0	17.733	15.164
$S=1$	0.1	4.357	2.715
	1.0	18.566	15.919
$S=2$	0.1	4.336	2.716
	1.0	20.911	18.221
$S=3$	0.1	4.413	2.716
	1.0	25.099	22.167

B. Electrons in a cavity

In Figs. 7–9, we further present our results of ECG calculations for $N=2$–4 electron systems formed and controlled by light-matter coupling. In these systems, we use a weak harmonic-oscillator confining potential ($\omega=0.1$ a.u.). Although this confinement allows the density to spread out far away from the center, the interaction of these systems with light strongly squeezes the density toward the center.

We test the systems for three different ω_p's (photon frequency) and different coupling strengths. The first strong coupling $\lambda=1$ confines the system into a $[-5, 5]$ a.u. box; the second moderate coupling $\lambda=0.1$ confines the system into a $[-10, 10]$ a.u. box; and the weakest $\lambda=0.01$ forces the system into a roughly $[-12, 12]$ a.u. box. Note that λ^2 appears in the dipole self-interaction term so the confinement caused by this term in the $\lambda<1$ cases is very weak. In this case, we do not make a comparison with DFT because the LDA-based DFT does not produce meaningful results. Only selected spin states are included, as others show similar density distributions.

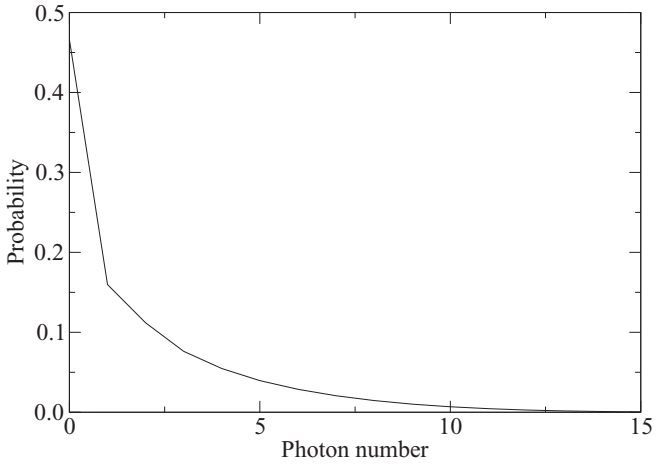

FIG. 6. Photon number as a function of the photon space for a single electron system with $\lambda=0.1$ a.u., and $\omega_p=0.1$ a.u.

Note that in this case, we are not merely dealing with a harmonic confinement as in the previous section, but as the wave function in Eq. (2.13) shows, the electrons are confined in different photon number spaces coupled to each other. The electron density is the sum of the electron density calculated in the orthogonal photon number spaces. An example is shown in Fig. 6 for a case of a single electron. The figure shows the probability of different photon number spaces, i.e., the fraction of the norm of the wave function belonging to different $|n\rangle$ in Eq. (2.13). In this one-electron case, the coupling is relatively strong; high photon spaces are coupled and less than 50 percent of the density is in the zero photon space.

Figure 7 shows the electron density of an $N=2$ system as a function of ω_p and λ. The coupling between different photon spaces is controlled by g [see Eq. (2.11)], and the strength of confinement in a given photon space is determined by λ. For a given λ value, the dependence on ω_p is relatively small because the coupling is proportional to $\sqrt{\omega_p}$. For a given ω_p, the positions and structures of the peaks are strongly dependent on λ. One significant difference between the harmonic confinement and the photon coupled case (Figs. 1 and 7) is that the density is much smaller between the peaks in the latter case.

Figures 8 and 9 show a similar dependence on ω_p for a given λ. The confinement is determined by λ and the density distributions have almost identical widths and peak positions. By increasing ω_p, the peak structure may become less emphasized for non-spin-polarized cases (e.g., for the $N=4$, $S=0$ case, only two or three peaks manifest for larger ω_p or λ). Similar to harmonic confinement, the number of the density peaks still matches with the number of electrons in spin-polarized cases.

For a given ω_p, the dependence on λ is strong (Figs. 7–9). Larger λ values make more compact systems. Overall, the λ dependence seems to be very similar in all cases. Photon spaces with small photon number ($n=0, 1, 2$) contain almost all the electron densities, even for stronger λ. The dependence of the densities and energies (see Supplemental Material [63]) on the photon frequency is moderate. The strong dependence

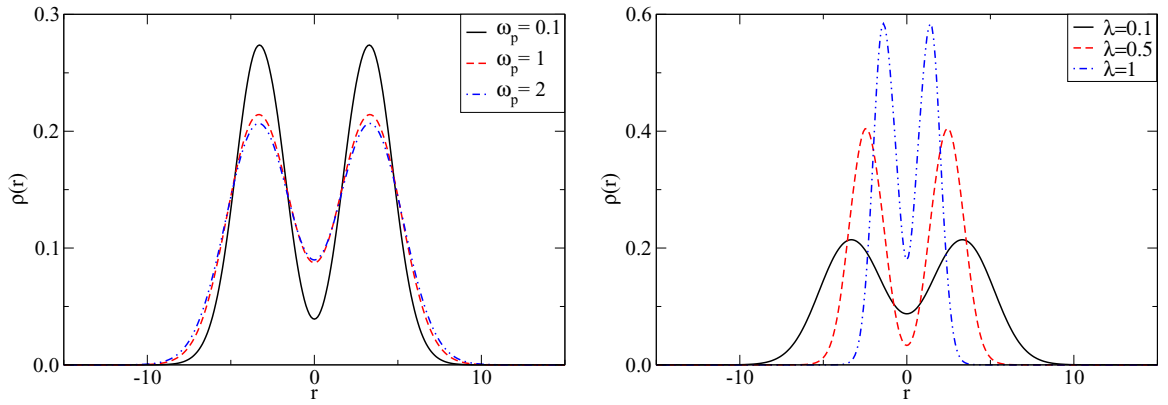

FIG. 7. Electron density of the two-electron $S = 1$ system coupled to light. Left: $\lambda = 0.1$ a.u.; right: $\omega_p = 1$ a.u. The distance r is in a.u.

on λ is due to two reasons. First, as Eq. (2.11) shows, the coupling is proportional to λ. Second and more importantly, the dipole self-interaction strength grows as λ^2. The latter fact also explains that for a given λ and changing ω (see Figs. 7–9), the spread of the density is nearly identical and only the relative heights of the peaks change. The dipole self-interaction term is responsible for squeezing the density toward the center.

These systems would not be bounded harmonically without an external confining potential. The photons couple to the electrons through the center-of-mass coordinate of the system [see Eqs. (2.10) and (2.12)]. The total wave function of the electrons can be factorized as a wave function of relative motion (depending on the relative coordinate) and the wave function of the center-of-mass motion (depending on X only). If there is no confinement, then the relative motion is governed by the repulsive Coulomb interaction and the system dissociates. The strength of the confinement, however, plays a very small role. Figure 10 shows three- and four-electron systems with a very weak confining potential for the spin-polarized ($S = 3/2$ and $S = 2$) cases. Without coupling, the density spreads out to 40 a.u. The coupling squeezes the density and the electrons form tightly localized electron peaks. These three- and four-electron densities are very similar to the $\omega = 0.1$ a.u. cases shown in Figs. 8 and 9.

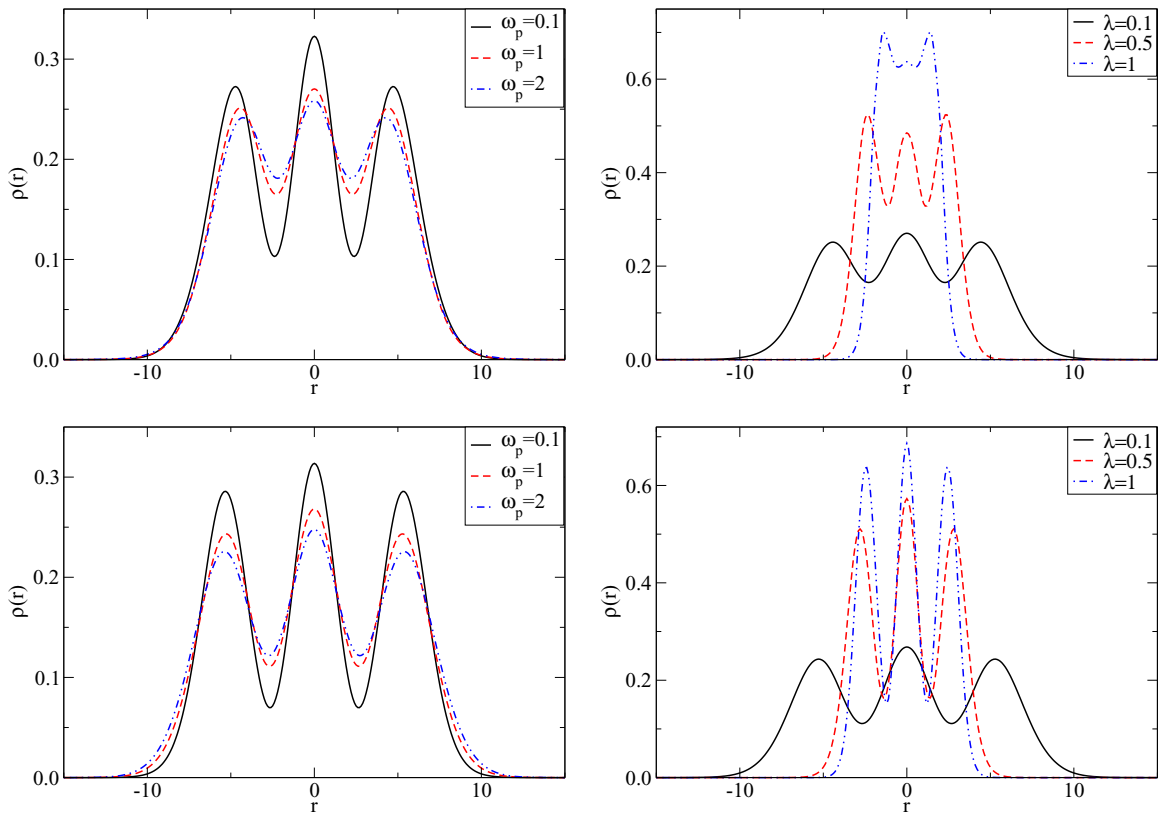

FIG. 8. Electron density of the three-electron system coupled to light. Top: $S = 1/2$; bottom: $S = 3/2$. Left: $\lambda = 0.1$ a.u.; right: $\omega_p = 1$ a.u. The distance r is in a.u.

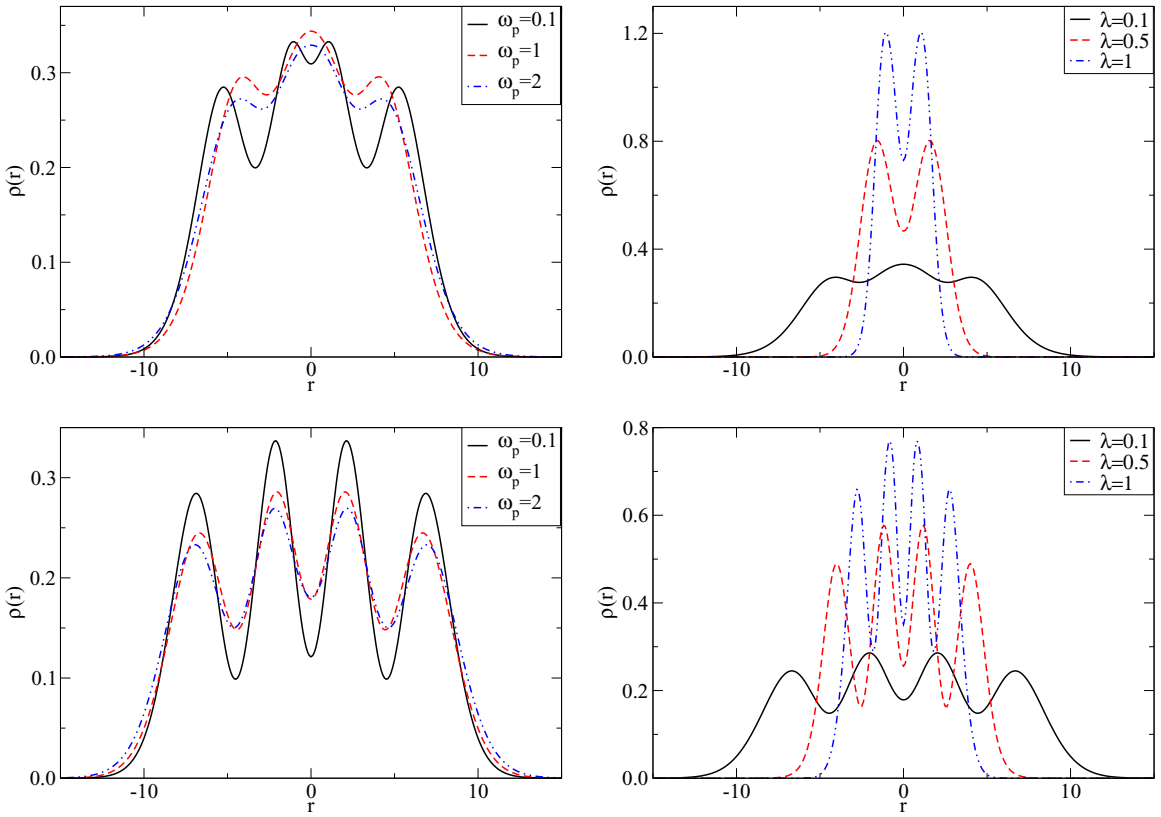

FIG. 9. Electron density of the four-electron system coupled to light. Top: $S = 0$; bottom: $S = 2$. Left: $\lambda = 0.1$ a.u.; right: $\omega_p = 1$ a.u. The distance r is in a.u.

IV. SUMMARY

1D few-electron systems are investigated using ECG basis functions. All matrix elements are analytically calculated and the basis parameters are optimized to generate flexible basis and accurate wave functions. $N = 2$–6 electron systems with different spin states are studied.

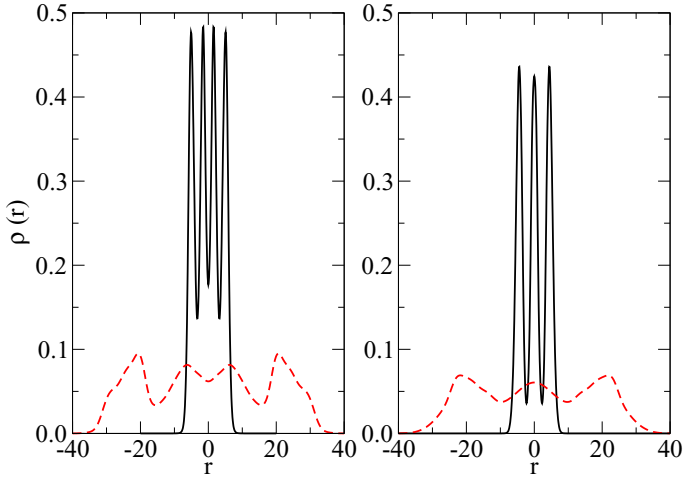

FIG. 10. Electron density of the four-electron (left) and three-electron (right) systems coupled to light. The solid line shows the density for $\lambda = 1.$ a.u., $\omega_p = 0.5$ a.u., and $\omega = 0.001$ a.u.; the dashed line shows the density without coupling. The distance r is in a.u.

Two different confinements are considered. In the first case, an external potential is used to localize the electrons. In the second case, there is a weak confining potential but the electrons are coupled to light and the dipole self-polarization determines the confinement. 1D Wigner crystal-like structures appear in both cases if the confinement or the coupling is very weak, and there is a similar tendency in the shape of the density as the confinement strength changes.

In spin-polarized cases, the number of density peaks is equal to the number of electrons because the shell structure, created by the confining potential, dominates. For non-spin-polarized cases, the number of peaks depends on the confinement strength and the total spin. This shows that one cannot identify the number of density peaks with the number of electrons in experiments. The symmetry of the few-electron wave function determines the number of peaks and the shape of the density. A direct comparison between the experiment [18] and theory is difficult because, in the experiment, the wave function of the electrons is three dimensional in the nanotube and fourfold degeneracy is present due to the valley and spin degrees of freedoms. The one-dimensional nature of the wave function of the electrons on the nanotube in the experiment, however, is likely to show the same properties as our calculated system.

We have shown that the crystal-like peak structure is also present in the case of strong confinement. These structures are not Wigner crystals because, in the strong confinement regime, the Coulomb interaction becomes negligible compared to the kinetic energy and the confinement. In this region,

in 1D, a shell structure is overwhelming and the nodes of the wave functions define the crystal-like peaks in the density.

Simpler models such as DFT-based calculations can capture the crystal-like peak structure in certain cases, especially for spin-polarized systems. Better exchange-correlation potentials can potentially extend the range of applications of the DFT-based approach to other cases. The advantage of the DFT is that it is easily applicable to much larger electron systems. The densities calculated by ECG can be used to create better exchange-correlation potentials for these 1D systems.

We have considered electrons with (soft) Coulomb interaction in this work, but other systems with repulsive interactions, such as degenerate Fermi gases in cavities [33], would be expected to show similar structures because the dipole self-interaction term presents a confinementlike potential for the particles.

Wigner crystals in systems confined by external potentials have already been observed [18]. The experimental realization of the light coupled systems might be possible by using nanotubes or optical lattices in cavities.

ACKNOWLEDGMENT

This work has been supported by the National Science Foundation (NSF) under Grant No. IRES 1826917.

[1] E. Wigner, Phys. Rev. **46**, 1002 (1934).
[2] C. C. Grimes and G. Adams, Phys. Rev. Lett. **42**, 795 (1979).
[3] Y. P. Monarkha and V. E. Syvokon, Low Temp. Phys. **38**, 1067 (2012).
[4] E. Y. Andrei, G. Deville, D. C. Glattli, F. I. B. Williams, E. Paris, and B. Etienne, Phys. Rev. Lett. **60**, 2765 (1988).
[5] A. Ghosal, A. D. Güçlü, C. J. Umrigar, D. Ullmo, and H. U. Baranger, Phys. Rev. B **76**, 085341 (2007).
[6] J. Cioslowski and K. Strasburger, J. Chem. Phys. **146**, 044308 (2017).
[7] C. Yannouleas and U. Landman, Rep. Prog. Phys. **70**, 2067 (2007).
[8] N. D. Drummond, Z. Radnai, J. R. Trail, M. D. Towler, and R. J. Needs, Phys. Rev. B **69**, 085116 (2004).
[9] S. M. Reimann, M. Koskinen, and M. Manninen, Phys. Rev. B **62**, 8108 (2000).
[10] C. Yannouleas and U. Landman, Phys. Rev. Lett. **82**, 5325 (1999).
[11] F. Pederiva, A. Emperador, and E. Lipparini, Phys. Rev. B **66**, 165314 (2002).
[12] S. M. Reimann and M. Manninen, Rev. Mod. Phys. **74**, 1283 (2002).
[13] M. Zarenia, D. Neilson, B. Partoens, and F. M. Peeters, Phys. Rev. B **95**, 115438 (2017).
[14] E. C. Regan, D. Wang, C. Jin, M. I. Bakti Utama, B. Gao, X. Wei, S. Zhao, W. Zhao, Z. Zhang, K. Yumigeta *et al.*, Nature (London) **579**, 359 (2020).
[15] H. Li, S. Li, E. C. Regan, D. Wang, W. Zhao, S. Kahn, K. Yumigeta, M. Blei, T. Taniguchi, K. Watanabe, S. Tongay, A. Zettl, M. F. Crommie, and F. Wang, Nature **597**, 650 (2021).
[16] Y. Liu, C. Zeng, J. Yu, J. Zhong, B. Li, Z. Zhang, Z. Liu, Z. M. Wang, A. Pan, and X. Duan, Chem. Soc. Rev. **50**, 6401 (2021).
[17] V. V. Deshpande and M. Bockrath, Nat. Phys. **4**, 314 (2008).
[18] I. Shapir, A. Hamo, S. Pecker, C. P. Moca, Ö. Legeza, G. Zarand, and S. Ilani, Science **364**, 870 (2019).
[19] S. Pecker, F. Kuemmeth, A. Secchi, M. Rontani, D. C. Ralph, P. L. McEuen, and S. Ilani, Nat. Phys. **9**, 576 (2013).
[20] G. Manna and M. K. Sanyal, Adv. Photon. Res. **2**, 2000039 (2021).
[21] D. D. Vu and S. Das Sarma, Phys. Rev. B **101**, 125113 (2020).
[22] M. Ostilli and C. Presilla, Phys. Rev. Lett. **127**, 040601 (2021).
[23] H. J. Schulz, Phys. Rev. Lett. **71**, 1864 (1993).
[24] L. Sárkány, E. Szirmai, C. P. Moca, L. Glazman, and G. Zaránd, Phys. Rev. B **95**, 115433 (2017).
[25] G. G. Spink, R. J. Needs, and N. D. Drummond, Phys. Rev. B **88**, 085121 (2013).
[26] D. Jost and M. W. C. Dharma-wardana, Phys. Rev. B **72**, 195315 (2005).
[27] F. H. Zong, C. Lin, and D. M. Ceperley, Phys. Rev. E **66**, 036703 (2002).
[28] G. Ortiz, M. Harris, and P. Ballone, Phys. Rev. Lett. **82**, 5317 (1999).
[29] N. T. Ziani, F. Cavaliere, K. G. Becerra, and M. Sassetti, Crystals **11**, 20 (2021).
[30] S. Blien, P. Steger, N. Hüttner, R. Graaf, and A. K. Hüttel, Nat. Commun. **11**, 1636 (2020).
[31] T. Cubaynes, M. R. Delbecq, M. C. Dartiailh, R. Assouly, M. M. Desjardins, L. C. Contamin, L. E. Bruhat, Z. Leghtas, F. Mallet, A. Cottet *et al.*, npj Quantum Inf. **5**, 47 (2019).
[32] W. C.-W. Huang, H. Batelaan, and M. Arndt, Phys. Rev. Lett. **126**, 253601 (2021).
[33] Q. Sun, X.-H. Hu, A.-C. Ji, and W. M. Liu, Phys. Rev. A **83**, 043606 (2011).
[34] L. Lacombe, N. M. Hoffmann, and N. T. Maitra, Phys. Rev. Lett. **123**, 083201 (2019).
[35] J. Flick, M. Ruggenthaler, H. Appel, and A. Rubio, Proc. Natl. Acad. Sci. **112**, 15285 (2015).
[36] J. Flick, M. Ruggenthaler, H. Appel, and A. Rubio, Proc. Natl. Acad. Sci. **114**, 3026 (2017).
[37] F. Buchholz, I. Theophilou, S. E. B. Nielsen, M. Ruggenthaler, and A. Rubio, ACS Photon. **6**, 2694 (2019).
[38] N. M. Hoffmann, L. Lacombe, A. Rubio, and N. T. Maitra, J. Chem. Phys. **153**, 104103 (2020).
[39] M. Ruggenthaler, N. Tancogne-Dejean, J. Flick, H. Appel, and A. Rubio, Nat. Rev. Chem. **2**, 0118 (2018).
[40] C. Schäfer, M. Ruggenthaler, H. Appel, and A. Rubio, Proc. Natl. Acad. Sci. **116**, 4883 (2019).
[41] J. Mitroy, S. Bubin, W. Horiuchi, Y. Suzuki, L. Adamowicz, W. Cencek, K. Szalewicz, J. Komasa, D. Blume, and K. Varga, Rev. Mod. Phys. **85**, 693 (2013).
[42] E. A. Power, S. Zienau, and H. S. W. Massey, Philos. Trans. R. Soc. London A **251**, 427 (1959).
[43] T. Zaklama, D. Zhang, K. Rowan, L. Schatzki, Y. Suzuki, and K. Varga, Few-Body Syst. **61**, 6 (2019).

[44] D. K. Zhang, D. W. Kidd, and K. Varga, Nano Lett. **15**, 7002 (2015).
[45] D. W. Kidd, D. K. Zhang, and K. Varga, Phys. Rev. B **93**, 125423 (2016).
[46] C. Riva, F. M. Peeters, and K. Varga, Phys. Rev. B **61**, 13873 (2000).
[47] K. Varga, Phys. Rev. Lett. **83**, 5471 (1999).
[48] J. Usukura, Y. Suzuki, and K. Varga, Phys. Rev. B **59**, 5652 (1999).
[49] K. Varga, P. Navratil, J. Usukura, and Y. Suzuki, Phys. Rev. B **63**, 205308 (2001).
[50] P. Hohenberg and W. Kohn, Phys. Rev. **136**, B864 (1964).
[51] W. Kohn and L. J. Sham, Phys. Rev. **140**, A1133 (1965).
[52] E. Räsänen, H. Saarikoski, V. N. Stavrou, A. Harju, M. J. Puska, and R. M. Nieminen, Phys. Rev. B **67**, 235307 (2003).
[53] H. Jiang, H. U. Baranger, and W. Yang, Phys. Rev. B **68**, 165337 (2003).
[54] K. Kärkkäinen, M. Koskinen, S. M. Reimann, and M. Manninen, Phys. Rev. B **70**, 195310 (2004).
[55] L. K. Castelano, G.-Q. Hai, B. Partoens, and F. M. Peeters, Phys. Rev. B **74**, 045313 (2006).
[56] M. Koskinen, M. Manninen, and S. M. Reimann, Phys. Rev. Lett. **79**, 1389 (1997).
[57] S. Pittalis and E. Räsänen, Phys. Rev. B **80**, 165112 (2009).
[58] V. Rokaj, D. M. Welakuh, M. Ruggenthaler, and A. Rubio, J. Phys. B: At. Mol. Opt. Phys. **51**, 034005 (2018).
[59] A. Mandal, S. Montillo Vega, and P. Huo, J. Phys. Chem. Lett. **11**, 9215 (2020).
[60] A. Mandal, T. D. Krauss, and P. Huo, J. Phys. Chem. B **124**, 6321 (2020).
[61] I. V. Tokatly, Phys. Rev. B **98**, 235123 (2018).
[62] J. P. Perdew and A. Zunger, Phys. Rev. B **23**, 5048 (1981).
[63] See Supplemental Material at http://link.aps.org/supplemental/10.1103/PhysRevA.104.043109 for calculations with other confinement potentials.
[64] P.-F. m. c. Loos, Phys. Rev. A **89**, 052523 (2014).
[65] P. Elliott, A. Cangi, S. Pittalis, E. K. U. Gross, and K. Burke, Phys. Rev. A **92**, 022513 (2015).